

Short communication

Synthesis of Bi-doped titanium oxide by chemical bath deposition for dye synthesized solar cell application

A.A. Kamble^a, A.L. Jadhav^b, V.B. Ghanwat^c, S.L. Jadhav^b, D.S. Gaikwad^d, J.D. Nadargi^e,
D.V. Bhuse^f, V.M. Bhuse^{a,*}

^a Rajaram College, Shivaji University, Kolhapur 416004, India

^b The Institute of Science, Dr. Homi Bhabha State University, Mumbai 400032, India

^c Department of Chemistry, Yashwantrao Chavan Institute of Science, Lead Institute, Karmaveer Bhaurao Patil University, Satara, Maharashtra 415001, India

^d Department of Chemistry, Vivekanand College, Kolhapur, Maharashtra, India

^e Department of Physics, Santosh Bhimrao Patil College, Mandrup, Solapur 413221, India

^f Government Institute of Science, Nagpur 440001, India



ARTICLE INFO

Keywords:

Chemical bath deposition

Bi-doped TiO₂

Solar Cell

Amorphous Rutile TiO₂

DSSC Solar cell

Doping

ABSTRACT

This study investigates the effect of different doping percentages of the Bismuth in TiO₂ nanocrystals on structural, morphological, and optical properties. The Bi-Doped titanium oxide was prepared by CBD method followed by sensitization by using natural dye (strawberry ink) and used for solar cell application. The structure analysis was carried out by using XRD technique and it reveals the presence of amorphous Rutile phase. The UV-Vis spectrum shows that at 0.25 to 1 % of Bi doping in TiO₂ the band gap of titanium oxide decreases from 2.8 to 3.52 eV, and the variable band gap is more suitable for solar cell application because it can absorb large span of solar spectrum. The morphological analysis was carried out by using a SEM it shows the presence of Aelurophil (small petal) like morphology. The surface roughness is studied by the AFM. The elemental composition is confirmed by using EDS and XPS analysis technique. The maximum efficiency is observed for the 1% Bi-doped Titanium trioxide which is 0.37 %.

1. Introduction

Accelerating depletion of fossil fuels and increase in environmental pollution attracted researches across the world to search for efficient energy generation technologies. The solar cell is a promising area of research among all efficient energy generation technologies due to direct conversion of sunlight into electricity energy [1]. In the recent few decades, the demand of renewable and clean solar energy has attracted research interest to produce energy, in particular photovoltaic system [2,3]. The current, high interest in the nanostructures of titanium oxide is being driven in part by the abundance of low-cost processing methods, which have been shown to impact the resultant morphology, and in part by the fact that a given technology device may perform better when built using a special morphology [4,5]. Titanium oxide exhibits three different phases rutile, anatase, and brookite. These phases show different characteristics due to titanium being a very interesting material for various applications. TiO₂ is widely used for solar cell applications [6–10] gas sensing applications [11,12] and energy storage

supercapacitor applications [13]. These three different titanium oxide phases are thermally more stable and they show the large active surface area of the materials. Also, TiO₂ is low cost, easy to synthesize and delivers good efficiency, due to these it is widely used which converts solar energy to electrical energy [14,15]. The treatment to the photoelectrode is also one of the best ways to enhance the performance of solar cell [16,17].

The solution-based techniques to deposit different thin films for solar cell application are appealing due to its simplicity, low cost and large-scale applications [18,19]. The chemical deposition method offers numerous advantages like low cost, low temperature deposition, environmentally friendly and most significantly no requirement of sophisticated equipment [20–22]. The doping of different elements in titanium oxide materials has been widely studied for solar cell application. In recent years, some researchers find that doping the TiO₂ film with metal ions could be a promising approach to improve the electrons transfer in the TiO₂-based nanostructured electrode of solar cell [23–27]. Lu et al. showed that, Nb-doped TiO₂ anatase crystalline nature and increases the

* Corresponding author.

E-mail address: vijaykbhuse13@gmail.com (V.M. Bhuse).

<https://doi.org/10.1016/j.inoche.2023.110681>

Received 8 December 2022; Received in revised form 27 March 2023; Accepted 31 March 2023

Available online 2 April 2023

1387-7003/© 2023 Elsevier B.V. All rights reserved.

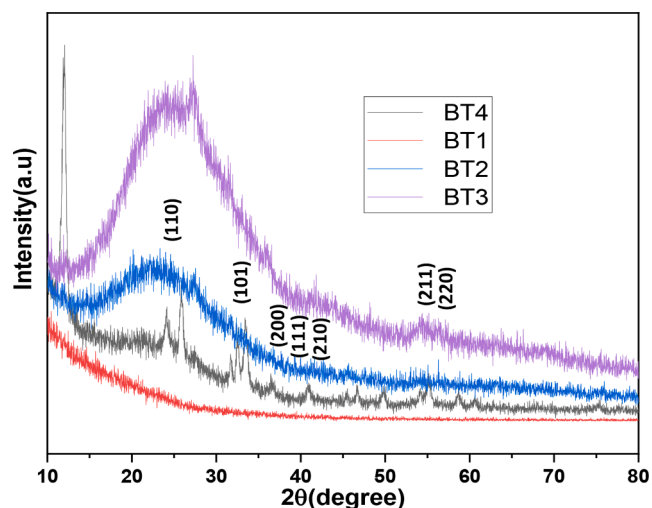


Fig. 1. XRD patterns of BT₁, BT₂, BT₃, and BT₄ Bi-doped TiO₂ samples (Indexing for BT₄).

performance of the conductivity with a positive shift in the potential band [28]. Kim et. al. prepared Cr-doped TiO₂ used for the photoanodes of DSSCs, and the enhanced performance is associated with the adjusting of the band structure of TiO₂ [29]. The doping of Bismuth is also one of the promising tasks to improve the solar cell performance and lots of reports have been shown the interesting results for it [30–34].

In the present work, we have successfully synthesized Bi doped TiO₂ nanomaterials using a simple and cost-effective chemical bath deposition method. The obtained nanomaterial was then annealed at 400 °C to evaluate the effect of Bi-doped titanium oxide on the DSSC application. The films were characterized to study the morphological nanostructure, crystallite structure, optical properties, compositional and I-V characteristics.

2. Experimental

The chemicals were used for the preparation of thin films are of standard grade which include, Bismuth nitrate (Bi(NO₃)₃) (Sigma Aldrich), Titanium chloride (TiCl₃) (Sigma Aldrich), and liquid Ammonia (NH₃) (Loba Chem). During preparation of all solutions of Bismuth doped Titanium oxide thin films distilled water were used. The thin films were deposited on to conducting FTO glass having dimensions of 75 × 25 × 1.35 mm. The cleaning of FTO slides was done by keeping them in a beaker containing distilled water and ultrasonicated for

sufficient time. Then rinsed with acetone and distilled water several times earlier to deposition of Bi-doped TiO₂ thin films.

2.1. Deposition of Bi doped TiO₂ thin films

To deposit different doping percentages of bismuth in TiO₂ thin films different molar concentrations of Bi(NO₃)₃ used in 50 ml TiCl₃ of solution. Further, the addition of 20 ml liquor NH₃ slowly drops by drop with constant stirring so as to obtain a stable complex. The NH₃ worked as a complexing agent in prepared solutions. Also, ammonia maintains the pH of the solution in the range of 9 to 11. Then in an oil bath, the beaker of the reaction solution was taken and then cleaned FTO glass slides were vertically positioned with the help of the substrate holder. The oil bath was then subjected to room temperature and wait for 3–4 Hr to get good deposition. The deposited samples at different doping concentrations of Bi(NO₃)₃ 0.25, 0.50, 0.75, and 1.00 M nomenclatures as BT₁, BT₂, BT₃, and BT₄ respectively. The percent doping was calculated to be 0.25, 0.50, 0.75 and 1% for BT₁, BT₂, BT₃, and BT₄ films respectively. After deposition time, it was observed that white coloured complete deposition on to the slides, was taken out, followed by washing with distilled water several times and drying at room temperature. After deposition annealing was carried out at 400 °C for 2 hr.

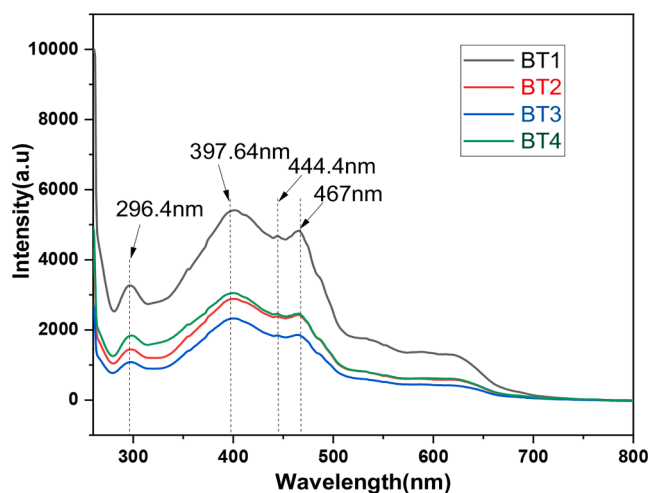


Fig. 3. Photo-Luminescence spectra of BT₁, BT₂, BT₃, and BT₄ Bi-doped TiO₂ samples.

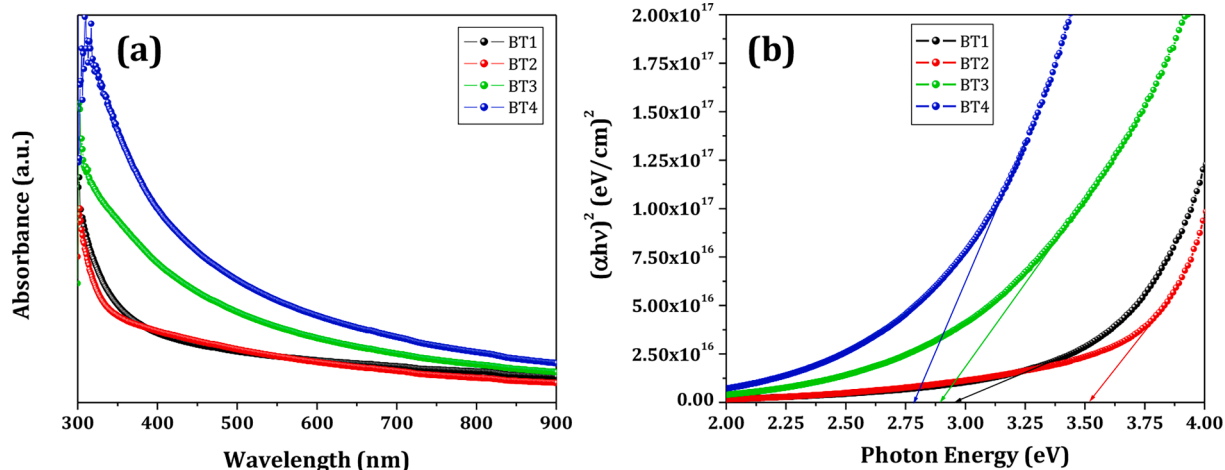


Fig. 2. UV-Vis absorbance (a) and Tauc plot showing band gap (b) of BT₁, BT₂, BT₃, and BT₄ Bi-doped TiO₂ samples.

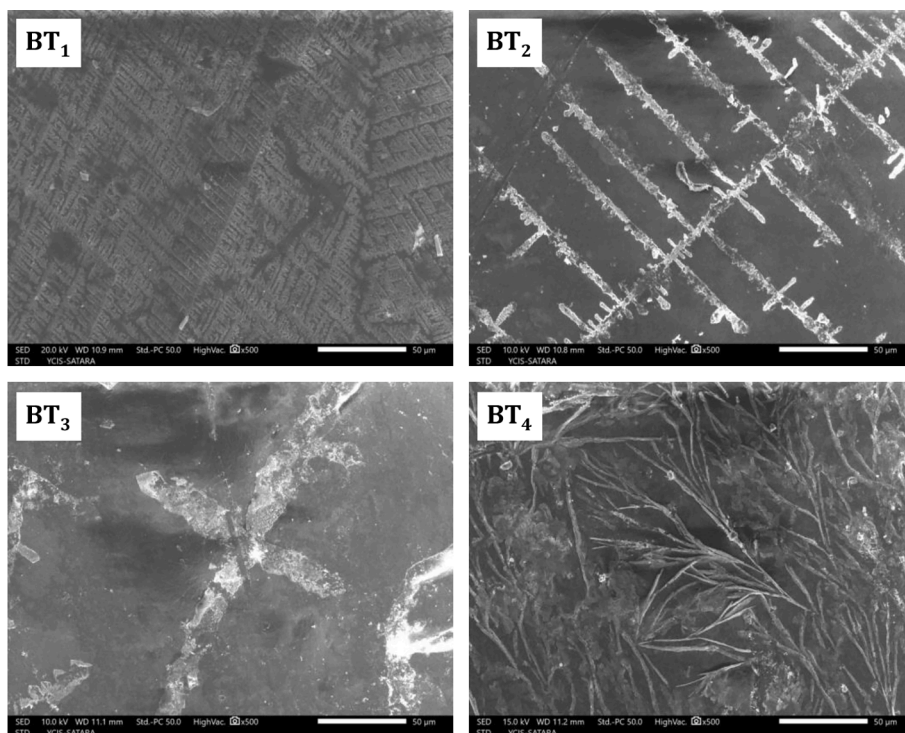


Fig. 4. SEM images of BT₁, BT₂, BT₃, and BT₄ Bi-doped TiO₂ samples.

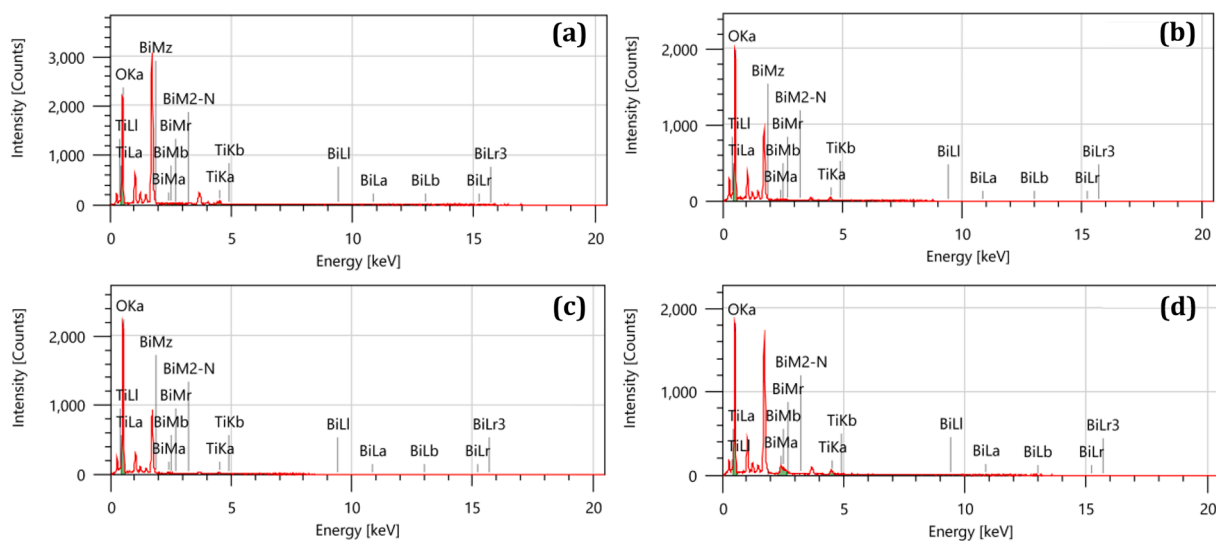


Fig. 5. EDS spectra of BT₁, BT₂, BT₃, and BT₄ Bi-doped TiO₂ samples showing presence of elements.

2.2. Fabrication of DSSCs device

Bi-doped TiO₂ photo anode electrode was soaked in natural dye (strawberry ink) solution for 2 h. After 2 h the prepared Bi-doped TiO₂ photo anode electrode was removed from the strawberry dye solution and washed several times in ethanol as the absorbed dye molecule was removed. Finally, we get the Dye sensitized Bi-doped TiO₂ photoanode electrode and used it as a counter electrode for the analysis of solar cells in the Platinum 1 M KI electrolyte.

3. Characterization

The structural analysis of prepared samples was carried out by using an X-ray diffraction (XRD) spectroscopy using Philips PW-1710

diffractometer with CuK α 1 ($\lambda = 1.54056 \text{ \AA}$) radiation with a diffraction angle (2θ) between the range of 10–80°. The analysis of optical absorption was carried out by using UV 3600 Shimadzu UV-VIS-NIR double beam spectrophotometer in the wavelength range 300–900 nm and Tauc plot was used to determine the band gap of films. The study of surface morphology was carried out by using Scanning electron microscopy (SEM) using Jeol JSM-IT-200. The surface roughness of the samples was carried out by using Atomic force microscope (AFM). To determine the exact oxidation states X-ray photoelectron spectroscopy (XPS) analysis was carried out. The solar cell analysis of prepared Bi-TiO₂ electrodes was carried out by using an electrochemical CH instrument (CHI 6F00E) using UV-Vis lamp using KI electrolyte.

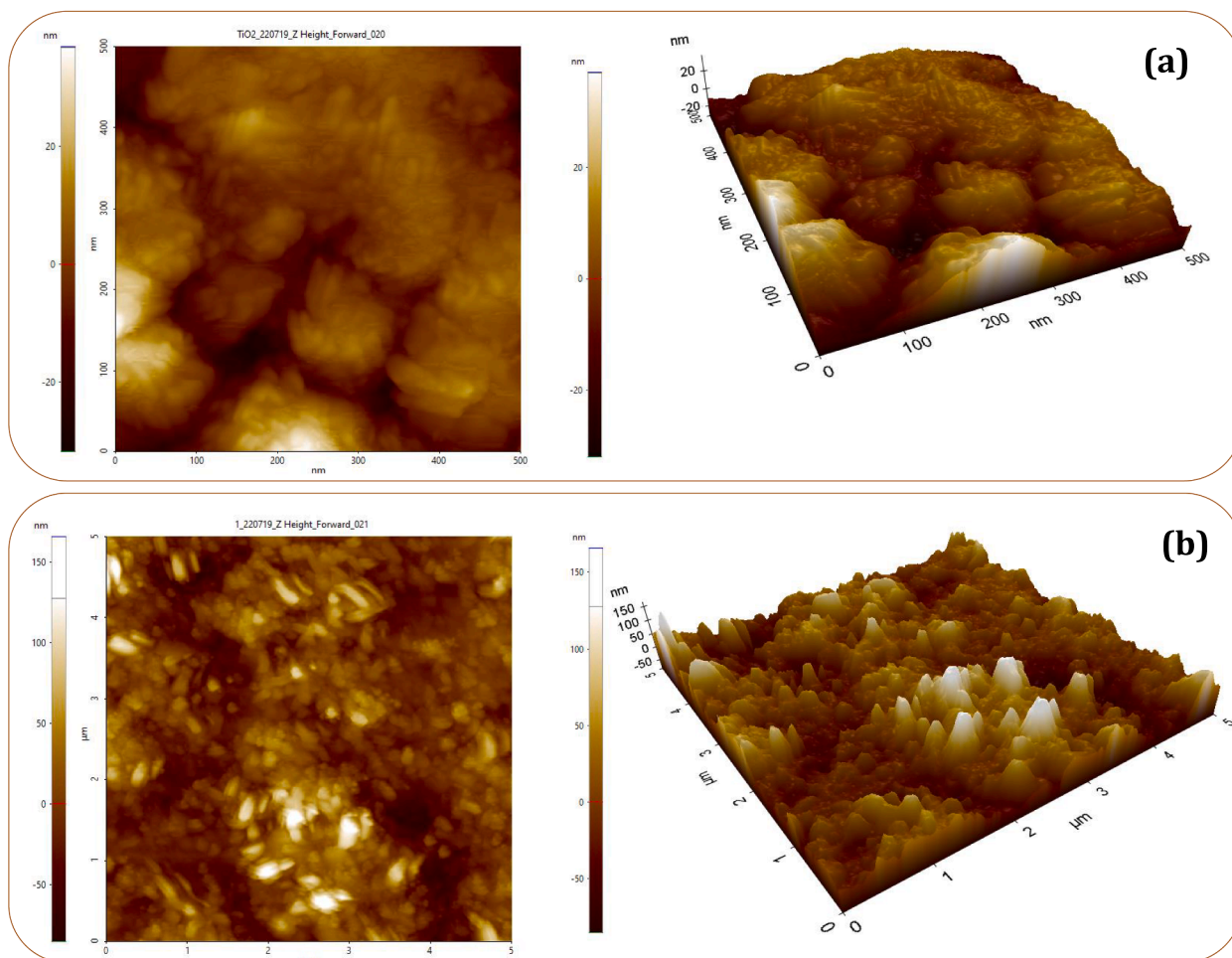


Fig. 6. 2D and 3D AFM images of TiO₂ and Bi doped TiO₂ material.

4. Results and discussion

4.1. XRD analysis of Bi-doped TiO₂ thin films

By XRD studies, we have been determined the structure of the Bi-doped TiO₂ nanomaterials. Fig. 1 shows the XRD patterns of the Bi-doped TiO₂ nanomaterials. The nature of pattern is somewhat amorphous and it matches the JCPDS standard card number 75–1537 of Bi-doped TiO₂ are of rutile phase [24]. Therefore, we can conclude that Bismuth has been effectively doped into the TiO₂ lattice. In general, as the doping concentration increases, the lattice parameters of the host change according to Vegard's law due to the generation of strain in the crystal lattice of the host material and the shift in diffraction peaks with regard to the ionic radius of the dopant. As a result, the presence of the Bi impurity may deteriorate the crystal quality which can be result in formation of amorphous nature of TiO₂ with doping concentration. In order to obtain the average crystallite size of Bi-doped TiO₂ nanomaterials, Debye–Scherrer equation was used [35]. The crystallite size for the major peak of the BT₁, BT₂, BT₃, and BT₄ evaluated is about 28, 30, 34, 36 nm respectively. As can be seen, the crystallite size of the TiO₂ increases with increasing the Bi doping concentration.

4.2. UV Vis spectroscopy analysis

UV–Vis spectroscopy is used to study the optical properties of film nanomaterials. The synthesized nanomaterials are dispersed in 10 ml of soluble liquid and further ultrasonic and the prepared sample solution is used for the analysis of the UV–Vis. Fig. 2 shows the optical absorption of

all Bi-doped TiO₂ nanomaterials. From the absorption spectrum it can be seen that, the absorption edge of doped TiO₂ nanomaterials appears at ~ 320 nm. The TiO₂ absorption edge significantly shifts to higher wavelength with increasing Bi dopant concentration in TiO₂. Similarly, light absorption in the UV–visible region increases with Bi concentration. The band gap of the synthesized nanomaterials is calculated by the Tauc relation. The observed band gaps for the BT₁, BT₂, BT₃, and BT₄ Bi-doped TiO₂ are 2.9, 3.52, 2.8, and 2.72 eV respectively. The optical band gap is initially higher but increases with Bi doping concentration and then decreases the band gap values. The decrease in the band gap with Bi doping concentration may be attributed due to, the localized states present near the valence band of the TiO₂ and the formation of colour centres, which are associated with the oxygen vacancies in TiO₂ or to the radicals in the titanium dioxide lattice associated with the doping ions [36].

4.3. PL analysis

The PL spectra of Bi-doped TiO₂ nanomaterials are shown in Fig. 3. From the graph, it is observed that the PL spectrum intensity is inversely related to the efficacy of the photocatalytic. This implies that the greater the PL intensity the greater will be the electron-hole pair recombination. This eventually decreases the photocatalytic process, due to the limited availability of the reactive radical intermediates. It is also observed that the emission peaks for the Bi-doped TiO₂ nanomaterials at 296.44, 397.4, 444.4, and 467 nm, show a weak intensity peak with increasing Bi doping content in TiO₂. The near band edge UV emission peaks at 296.4 to 397.4 nm correspond to the recombination of electron-hole

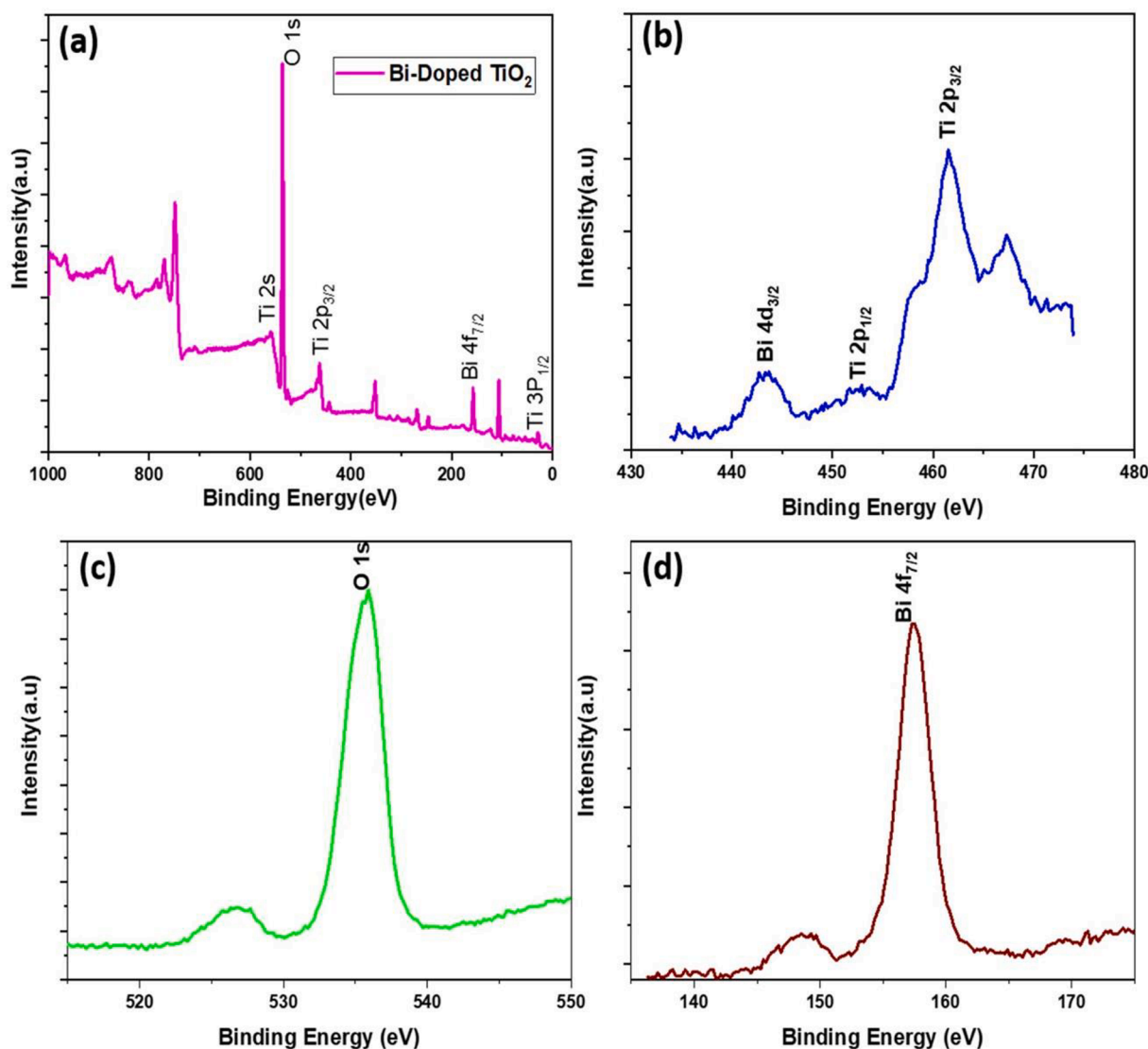


Fig. 7. XPS analysis of Bi doped TiO_2 , the survey spectrum (a), core level spectrum of $\text{Ti}2p$ peak (b), core level spectra of $\text{O}1s$ peak (c) and core level spectrum of $\text{Bi}4f$ peak (d).

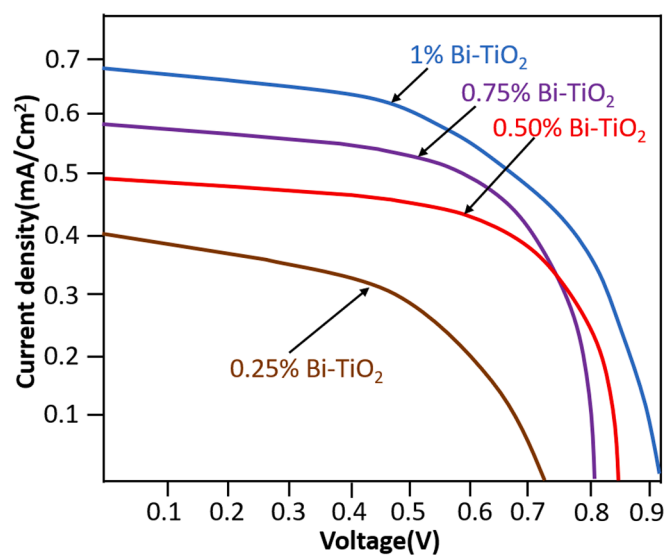


Fig. 8. I-V Characteristics of DSSCs of BT_1 , BT_2 , BT_3 , and BT_4 Bi-doped TiO_2 .

Table 1

Calculated values achieved from the J-V curves of each solar cell.

Samples	V_{oc} (mV)	I_{sc} (mA)	FF	Efficiency (%)
BT_1	0.73	0.41	0.51	0.15
BT_2	0.84	0.49	0.74	0.31
BT_3	0.81	0.58	0.62	0.30
BT_4	0.92	0.68	0.55	0.37

pairs in the range. The broad emission band in the visible region at 444.4 nm is due to the interstitial vacancies in the TiO_2 lattice framework [37].

4.4. SEM and EDS analysis

Fig. 4 shows the SEM images of the synthesized Bi-doped TiO_2 thin film nanomaterials. The morphology of Bi-doped TiO_2 nanomaterials is a regular line manner to Aeluropuslogophiles (small petal). In addition, the aggregation of nanoparticles also observed in SEM images of the samples. Regarding the results of the XRD experiment, it can be inferred that the size of crystallites in the nanoparticles is apparently less than the size of the nanoparticles which indicates that the produced particles are

in the nanocrystalline phase. The crystallite is the smallest uniform crystallographic unit which is based on the disorientation of its neighbours. The particle consists more crystallite which are in different orientations. XRD gives the crystallite size which is very small, not the particle size which is greater than crystallite. The BT₄ material shows the highest roughness which may be fruitful for the solar cell application. As the sample poses rougher surface it consists more surface area which enhances the solar cell performance [38]. Fig. 5 shows the elemental composition of the Bi-doped TiO₂. The presence of peak at 4.508, 10.837 and 0.525 KeV confirms the presence of Ti, Bi and O in samples respectively. From now it is clearly observed that the Bi is successfully doped in TiO₂. To confirm the oxidation state representative same further analyzed by XPS.

4.5. AFM analysis

Fig. 6 shows the AFM studies of bare TiO₂ and representative Bi doped TiO₂ thin films. Here, we observed that the roughness of sample increases after doping and which increases up to 25.7 nm. The 2D (5 × 5 nm) and 3D (5 × 5 nm) AFM images clearly shows the rough surface of the Bi doped TiO₂ nanomaterials. The rough surface is beneficial for the electrolyte to disperse well and to get maximum surface area of photocatalyst.

4.6. X-Ray photoelectron spectroscopy analysis

The chemical composition of the elements and its oxidation states in the Bi doped TiO₂ optimized materials were analysed using the XPS technique. The XPS survey spectrum data in the Fig. 7(a) reveals that the existence of Ti2s, Ti2p, O1s, C2p, Bi4f and Ti3p elemental oxidation states. Fig. 7(b) shows the XPS spectra of TiO₂ is Ti2s, Ti2p, and Ti3p respectively with their corresponding binding energy. The Ti 2p spectrum shows the two excitation peaks sited at 453 eV and 462 eV binding energies [39]. The deconvolution peaks in the Titanium spectrum give spin energy splitting value of 9 eV between two states binding energies 453 eV and 462 eV. The observed peak O1s at the binding energies of 535.5 eV, shown in Fig. 5 (c) and consistent with the literature reports [40]. The Bismuth nanomaterials shows the two peaks at 157.4 eV and 443.2 eV binding energy, similarly results represented by Kumar et al. [41]. The results confirmed that the prepared Bi doped TiO₂ nanomaterial is successfully formed on to the thin films.

4.7. I-V characteristics of DSSCs measurement

Fig. 8 shows the I-V characteristics of each solar cell consisting of dye-sensitized different doping percentages of Bi-doped TiO₂ film anode electrode. The parameter of the I-V is the change in short circuit current density (J_{sc}), open circuit potential (V_{oc}), and conversion efficiency, which is related to the doping concentration of the bismuth in titanium trioxide. The SEM and AFM characteristics shows that the larger surface area of the prepared 1% Bi-doped TiO₂ nanomaterials has more rough surface due to which the redox couple could diffuse more effectively than other Bi-doped TiO₂ samples. Consequently, the nanoparticles show maximum short current density (J_{sc}). Although it was expected that smaller nanoparticle size could adsorb more active dye due to their greater active surface area of the thin film, it was shown that the small nanoparticles then active site space available to have better dye absorption due to the successful diffusion of the electrolytes to resultant in enhancement in the overall light conversion efficiency. The increasing dopant Bi-concentration in titanium oxide with the overall light conversion efficiency was observed to be 0.15, 0.31, 0.30, and 0.37 % for BT₁, BT₂, BT₃, and BT₄ respectively. All the achieved values from the J-V curves of each DSSCs solar cell are shown in Table 1.

5. Conclusions

The Bi-doped TiO₂ nanomaterials as a working electrode for DSSC have been successfully prepared by a simple and efficient CBD method. The prepared Bi-doped TiO₂ shows an increasing percentage of Bi content in the titanium oxide shows crystalline nature. The observed band gap was 2.8 eV at 1% Bi-doped Titanium oxide, which was minimum than other electrodes. The SEM morphology of the thin films observed a small petal-like structure. The optimized Bi doped TiO₂ shows surface roughness of 25.7 nm. The EDS and XPS confirmed the chemical composition of the Bi Doped TiO₂. The Bi-doped TiO₂ thin film electrode was sensitized with natural strawberry dye. The 1% Bi - TiO₂ electrode with DSSC cell shows best performance than the other DSSC. The observed maximum efficiency of the DSSC is 0.37 % with FF is 0.55.

Declaration of Competing Interest

The authors declare that they have no known competing financial interests or personal relationships that could have appeared to influence the work reported in this paper.

Data availability

No data was used for the research described in the article.

References

- [1] M. Maaza, B.D. Ngom, Z.Y. Nuru, S. Khamlich, Surface-Interface Investigation and Stability of Cermet-Based Solar Absorbers by Grazing Angle X-Rays Reflectometry: Pt-Al₂O₃ Case, Arab. J. Sci. Eng. 39 (2014) 5825–5846, <https://doi.org/10.1007/s13369-014-1110-y>.
- [2] S.S. Patil, K.V. Khot, R.M. Mane, P.N. Bhosale, Novel hydrothermal route for synthesis of photoactive Cu₂ZnSn(S, Se)₄ nanocrystalline thin film: efficient photovoltaic performance, J. Mater. Sci. Mater. Electron. 31 (2020) 5441–5451, <https://doi.org/10.1007/s10854-020-03107-1>.
- [3] V.B. Ghanwat, S.S. Mali, C.S. Bagade, R.M. Mane, C.K. Hong, P.N. Bhosale, Thermoelectric Properties of Indium(III)-Doped Copper Antimony Selenide Thin Films Deposited Using a Microwave-Assisted Technique, Energy Technol. 4 (2016) 835–842, <https://doi.org/10.1002/ente.201500508>.
- [4] S.S. Patil, S.S. Mali, C.K. Hong, P.N. Bhosale, Designing of novel efficient photoactive ternary Zn_{1-x}Cu_xSe thin film materials via hydrothermal route: Photoelectrochemical (PEC) cell study, Mater. Sci. Semicond. Process. 105 (2020), 104727, <https://doi.org/10.1016/j.mssp.2019.104727>.
- [5] L. Kotsedi, Z.Y. Nuru, P. Mthunzi, T.F.G. Muller, S.M. Eaton, B. Julies, E. Manikandan, R. Ramponi, M. Maaza, Femtosecond laser surface structuring and oxidation of chromium thin coatings: Black chromium, Appl. Surf. Sci. 321 (2014) 560–565, <https://doi.org/10.1016/j.apsusc.2014.09.168>.
- [6] Y. Akila, N. Muthukumarasamy, D. Velauthapillai, TiO₂-based dye-sensitized solar cells, in: Nanomater. Sol. Cell Appl., Elsevier, 2019: pp. 127–144. 10.1016/B978-0-12-813337-8.00005-9.
- [7] R.S. Dubey, S.R. Jadhav, A.B. Bhorde, Synthesis and Characterization of Various Doped TiO₂ Nanocrystals for Dye-Sensitized Solar Cells, ACS Omega. 6 (2021) 3470–3482, <https://doi.org/10.1021/acsomega.0c01614>.
- [8] A.A. Kamble, P.A. Ubale, A.L. Jadhav, S.L. Jadhav, A.V. Kadam, C.M. Kanamadi, V. M. Bhuse, Studies on Optical, Structure, and Photoconductivity of Titanium Dioxide Thin Films Prepared by Chemical Bath Deposition Via Aqueous Route, Macromol. Symp. 400 (2021), <https://doi.org/10.1002/masy.202100020>.
- [9] B. Roose, S. Pathak, U. Steiner, Doping of TiO₂ for sensitized solar cells, Chem. Soc. Rev. 44 (2015) 8326–8349, <https://doi.org/10.1039/c5cs00352k>.
- [10] O.B. Qader, Y. Ruisheng, K. Chaudhary, F.F. Muhammad, M.Y. Yahya, M. R. Ahmad, F.D. Ismail, J. Ali, TiO₂ doped nanocomposite thin film for photovoltaic application, Dig. J. Nanomater. Biostructures. 15 (2020) 25–32.
- [11] Y. Wang, T. Wu, Y. Zhou, C. Meng, W. Zhu, L. Liu, TiO₂-based nanoheterostructures for promoting gas sensitivity performance: Designs, developments, and prospects, Sensors (Switzerland). 17 (2017), <https://doi.org/10.3390/s17091971>.
- [12] A. Hodaie, A.S. Dezfali, H.R. Naderi, A high-performance supercapacitor based on N-doped TiO₂ nanoparticles, J. Mater. Sci. Mater. Electron. 29 (2018) 14596–14604, <https://doi.org/10.1007/s10854-018-9595-x>.
- [13] D.A.H. Hanaor, C.C. Sorrell, Review of the anatase to rutile phase transformation, J. Mater. Sci. 46 (2011) 855–874, <https://doi.org/10.1007/s10853-010-5113-0>.
- [14] J. Jaćimović, C. Vajur, R. Gaál, A. Magrez, H. Berger, L. Forró, High-pressure study of anatase TiO₂, Materials (Basel). 3 (2010) 1509–1514, <https://doi.org/10.3390/ma3031509>.
- [15] H. Imahori, S. Hayashi, T. Umeyama, S. Eu, A. Oguro, S. Kang, Y. Matano, T. Shishido, S. Ngamsinlapasathian, S. Yoshikawa, Comparison of electrode structures and photovoltaic properties of porphyrin-sensitized solar cells with TiO₂ and Nb, Ge, Zr-added TiO₂ composite electrodes, Langmuir. 22 (2006) 11405–11411, <https://doi.org/10.1021/la061527d>.

- [16] A. Karoro, Z.Y. Nuru, L. Kotsedi, K. Bouziane, B.M. Mothudi, M. Maaza, Selective Solar Absorbers' Properties of Laser Treated Electrodeposited Tubular Co-Al₂O₃ Nanocomposites, in, *Mater. Today Proc.*, Elsevier (2015) 4028–4037, <https://doi.org/10.1016/j.matpr.2015.08.032>.
- [17] L. Kotsedi, P. Sechogela, S.M. Eaton, A.G. Demir, F. Franceschini, B. Previtali, R. Ramponi, H.C. Swart, M. Maaza, Metal and Metal Oxide Transformation and Texturing Using Pulsed Fiber Laser, *Mater. Today Proc.* 2 (2015) 3950–3956, <https://doi.org/10.1016/J.MATPR.2015.08.024>.
- [18] S.S. Patil, R.M. Mane, S.S. Mali, C.K. Hong, P.N. Bhosale, Facile designing and assessment of photovoltaic performance of hydrothermally grown kesterite Cu₂ZnSnS₄ thin films: Influence of deposition time, *Sol. Energy.* 201 (2020) 102–115, <https://doi.org/10.1016/J.SOLENER.2020.02.089>.
- [19] S.S. Patil, K.V. Khot, S.S. Mali, C. Kook Hong, P.N. Bhosale, Investigating the Role of Selenium-Ion Concentration on Optoelectronic Properties of the Cu₂ZnSn (S_{1-x}Se_x)₄ Thin Films, *Ind. & Eng. Chem. Res.* 59 (2020) 10868–10881, <https://doi.org/10.1021/acs.iecr.0c00294>.
- [20] C.S. Bagade, V.B. Ghanwat, E. Van Keuren, P.N. Bhosale, A robust and self-assembled route to synthesis of CdZn(Sn_{1-x}Te_x)₂ photoanodes as light harvesters for photoelectrochemical solar cells, *J. Mater. Sci. Mater. Electron.* 29 (2018) 11763–11773, <https://doi.org/10.1007/s10854-018-9275-x>.
- [21] V.B. Ghanwat, S.S. Mali, C.S. Bagade, K.V. Khot, N.D. Desai, C.K. Hong, P. N. Bhosale, Enhancement in thermoelectric performance of Cu₃SbSe₄ thin films by In(III) doping; synthesized by arrested precipitation technique, *J. Mater. Sci. Mater. Electron.* 29 (2018) 8793–8800, <https://doi.org/10.1007/s10854-018-8896-4>.
- [22] X. Xu, Y. Ge, H. Wang, B. Li, L. Yu, Y. Liang, K. Chen, F. Wang, Sol-gel synthesis and enhanced photocatalytic activity of doped bismuth tungsten oxide composite, *Mater. Res. Bull.* 73 (2016) 385–393, <https://doi.org/10.1016/j.materresbull.2015.09.024>.
- [23] I. Ali, S. Kim, S. Kim, J. Kim, Anodization of bismuth doped TiO₂ nanotubes composite for photocatalytic degradation of phenol in visible light, *Catal. Today.* (2016), <https://doi.org/10.1016/j.cattod.2016.03.029>.
- [24] H. Li, J. Liu, J. Qian, Q. Li, J. Yang, Preparation of Bi-doped TiO₂ nanoparticles and their visible light photocatalytic performance, *Cuihua Xuebao/Chinese, J. Catal.* 35 (2014) 1578–1589, [https://doi.org/10.1016/S1872-2067\(14\)60124-8](https://doi.org/10.1016/S1872-2067(14)60124-8).
- [25] S. Bagwasi, B. Tian, J. Zhang, M. Nasir, Synthesis, characterization and application of bismuth and boron Co-doped TiO₂: A visible light active photocatalyst, *Chem. Eng. J.* 217 (2013) 108–118, <https://doi.org/10.1016/j.cej.2012.11.080>.
- [26] Y. Hu, Y. Cao, P. Wang, D. Li, W. Chen, Y. He, X. Fu, Y. Shao, Y. Zheng, A new perspective for effect of Bi on the photocatalytic activity of Bi-doped TiO₂, *Appl. Catal. B Environ.* 125 (2012) 294–303, <https://doi.org/10.1016/j.apcatb.2012.05.040>.
- [27] S. Murcia-López, M.C. Hidalgo, J.A. Navío, Synthesis, characterization and photocatalytic activity of Bi-doped TiO₂ photocatalysts under simulated solar irradiation, *Appl. Catal. A Gen.* 404 (2011) 59–67, <https://doi.org/10.1016/j.apcata.2011.07.008>.
- [28] X. Lü, X. Mou, J. Wu, D. Zhang, L. Zhang, F. Huang, F. Xu, S. Huang, Improved-Performance Dye-Sensitized solar cells using Nb-Doped TiO₂ electrodes: Efficient electron Injection and transfer, *Adv. Funct. Mater.* 20 (2010) 509–515, <https://doi.org/10.1002/adfm.200901292>.
- [29] C. Kim, K.S. Kim, H.Y. Kim, Y.S. Han, Modification of a TiO₂ photoanode by using Cr-doped TiO₂ with an influence on the photovoltaic efficiency of a dye-sensitized solar cell, *J. Mater. Chem.* 18 (2008) 5809–5814, <https://doi.org/10.1039/b805091k>.
- [30] N.C. Miller, M. Bernechea, Research Update: Bismuth based materials for photovoltaics, *APL Mater.* 6 (2018), <https://doi.org/10.1063/1.5026541>.
- [31] Z. Guo, P. Li, H. Che, G. Wang, C. Wu, X. Zhang, J. Mu, One-dimensional spindle-like BiVO₄/TiO₂ nanofibers heterojunction nanocomposites with enhanced visible light photocatalytic activity, *Ceram. Int.* 42 (2016) 4517–4525, <https://doi.org/10.1016/j.ceramint.2015.11.142>.
- [32] V.L. Chandraboss, J. Kamalakkannan, S. Senthilvelan, Synthesis of activated charcoal supported Bi-doped TiO₂ nanocomposite under solar light irradiation for enhanced photocatalytic activity, *Appl. Surf. Sci.* 387 (2016) 944–956, <https://doi.org/10.1016/j.apsusc.2016.06.110>.
- [33] A.M. Luís, M.C. Neves, M.H. Mendonça, O.C. Monteiro, Influence of calcination parameters on the TiO₂ photocatalytic properties, *Mater. Chem. Phys.* 125 (2011) 20–25, <https://doi.org/10.1016/j.matchemphys.2010.08.019>.
- [34] J. Xu, M. Chen, D. Fu, Study on highly visible light active Bi-doped TiO₂ composite hollow sphere, *Appl. Surf. Sci.* 257 (2011) 7381–7386, <https://doi.org/10.1016/j.apsusc.2011.02.030>.
- [35] M. Asemi, M. Ghanaatshoar, Preparation of CuCrO₂ nanoparticles with narrow size distribution by sol-gel method, *J. Sol-Gel Sci. Technol.* 70 (2014) 416–421, <https://doi.org/10.1007/s10971-014-3298-4>.
- [36] M. Asemi, M. Ghanaatshoar, Controllable growth of vertically aligned Bi-doped TiO₂ nanorod arrays for all-oxide solid-state DSSCs, *Appl. Phys. A Mater. Sci. Process.* 122 (2016), <https://doi.org/10.1007/s00339-016-0389-9>.
- [37] K. Bandopadhyay, J. Mitra, Zn interstitials and O vacancies responsible for n-type ZnO: what do the emission spectra reveal? *RSC Adv.* 5 (2015) 23540–23547, <https://doi.org/10.1039/c5ra00355e>.
- [38] A. Karoro, Z.Y. Nuru, L. Kotsedi, K. Bouziane, B.M. Mothudi, M. Maaza, Laser nanostructured Co nanocylinders-Al₂O₃ cermets for enhanced & flexible solar selective absorbers applications, *Appl. Surf. Sci.* 347 (2015) 679–684, <https://doi.org/10.1016/J.APSUSC.2015.04.098>.
- [39] A. Wiatrowski, M. Mazur, A. Obstarczyk, D. Wojcieszak, D. Kaczmarek, J. Morgiel, D. Gibson, Comparison of the physicochemical properties of TiO₂ thin films obtained by magnetron sputtering with continuous and pulsed gas flow, *Coatings.* 8 (2018), <https://doi.org/10.3390/COATINGS8110412>.
- [40] J. Du, G. Zhao, Y. Shi, Y. Haoyang, G. Li, Y. Zhu, R. Mao, W.W. Sa, A facile method for synthesis of N-doped TiO₂ nanooctahedra, nanoparticles, and nanospheres and enhanced photocatalytic activity, *Appl. Surf. Sci.* 273 (2013) 278–286, <https://doi.org/10.1016/j.apsusc.2013.02.032>.
- [41] P. Kumar, J. Singh, A.C. Pandey, Rational low temperature synthesis and structural investigations of ultrathin bismuth nanosheets, *RSC Adv.* 3 (2013) 2313–2317, <https://doi.org/10.1039/c2ra21907g>.